Synergistic Effects of Metal-Modified Carbon Nanotubes: Experimental Characterization and Theoretical Modeling for Energy and Environmental Solutions

Govindhasamy Murugadoss[a,*], Nachimuthu Venkatesh[a], Narthana Kandhasamy[a], Irina Zaporotskova[b], Durai Govindarajan[c], Natesan Kumaresan[d], Kamalan Kirubaharan[e], Uday Kumar Khanapuram[f*], Soorathep Kheawhom[c,*]

[a]*Centre for Nanoscience and Nanotechnology, Sathyabama Institute of Science and Technology (Deemed to be University), Chennai, Tamil Nadu 600 119, India*

[b]*Volgograd State University, 100 University Ave., Volgograd, 400062, Russia*

[c]*Department of Chemical Engineering, Faculty of Engineering, Chulalongkorn University, Bangkok 10330, Thailand*

[d]*Department of Physics, SSN Research Centre, Sri Sivasubramaniya Nadar College of Engineering, Chennai, 603110, Tamil Nadu, India*

[e]*Coating Department FunGlass – Centre for Functional and Surface Functionalized Glass, Alexander Dubcek University of Trencin 91150, Slovakia*

[f]*Energy Materials and Devices (EMD) Laboratory, Department of Physics, National Institute of Technology, Warangal 506004, Telangana, India.*

S.1 Electrode Fabrication for Water Splitting

The electrochemical experiments were carried out in a three-electrode cell configuration with a Pt counter electrode, an Ag/AgCl reference electrode, and active materials as a working electrode in a 6 M KOH aqueous solution. Nickel foam coated with CNT-based metal samples served as a working electrode. Cyclic voltammetry (CV), galvanostatic charge/discharge tests (GCD), and electrochemical impedance spectroscopy (EIS) were carried out on nickel foam substrates with a three-electrode configuration (BIOLOGIC). The nickel foam (NF) substrates were first cleaned with deionized water, then etched in a 0.1 M HCl solution at ambient temperature for 15 minutes before being rinsed with deionized water in an ultrasonic bath for 30 minutes. The mass of the electrodes was determined using an ultra-microbalance. Each electrode was manufactured with approximately 3 mg of electroactive material. Electroactive materials are prepared by mixing active materials, carbon black, and poly(vinylidene difluoride) (PVDF) with N-methylpyrrolidone (NMP) solvent. The resultant slurry was ultrasonically homogenised and coated on an NF, which was then dried in a vacuum oven at 80°C for 2 hours. CV readings were examined at sweep rates ranging from 5 to 100 mV s-1, with a potential window of 0 to 0.6 V, and GCD tests were performed at various current densities. Electrochemical impedance spectroscopy (EIS) was performed at frequencies ranging from 100 kHz to 0.01 Hz, with an amplitude of 10 mV.

S.2 Electrode Fabrication for Supercapacitor

The electrochemical measurements were performed utilising a three-electrode cell configuration with Pt as the counter electrode, Ag/AgCl as the reference electrode, and the synthesised materials as the working electrode, all immersed in a 6 M KOH aqueous electrolyte. The nickel foam (NF) substrates underwent initial cleaning with deionized (DI) water, followed by etching in a 0.1 M HCl solution at room temperature for 15 min. Subsequently, rinsing with DI water in an ultrasonic bath for 30 min. The electrode mass was

determined using an ultra-microbalance. The NF coated with K1 to K7 samples were used as a working electrode (The nickel foam serves as a current collector). Each fabricated electrode contained 3 mg of electroactive material.

The preparation of electroactive materials includes: mixing active materials, carbon black and poly(vinylidene difluoride) (PVDF) with N-methylpyrolidinone (NMP) solvent. The resultant slurry was homogenised via ultrasonication and then coated onto an NF, followed by drying at 80 ℃ for 2 hours in a vacuum oven. Cyclic voltammetry (CV), galvanostatic charge/discharge (GCD), and electrochemical impedance spectroscopy (EIS) were performed on NF substrates using a three-electrode setup (BIOLOGIC). The CV readings were examined using sweep rates ranging from 5 to 100 mV s-1 and a potential window of 0 to 0.6 V. The GCD tests were carried out at varying current densities. Meanwhile, electrochemical impedance spectroscopy (EIS) was performed within a frequency range of 100 kHz to 0.01 Hz with an amplitude of 10 mV. From the CV profiles, the specific capacitance (SC) was determined using Eqn **1**.

$$SC = \frac{1}{v \times (\Delta V) \times m} \int_{Vi}^{Vf} I(V)dV \qquad (1)$$

where SC stands for specific capacitance (F g^{-1}), m indicates the mass loading of the active material, v is the scan rate (mV s^{-1}), ΔV denote potential window, and $\int_{Vi}^{Vf} I(V)dV$ refers to the integral area under the CV curve. Also, Eqn **2** was utilised to analyse the SC through the utilisation of GCD curves and discharge time (td).

$$Cs = \frac{I \times \Delta t}{m \times \Delta V} \qquad (2)$$

Where I stand for current density (A), Δt for GCD curve discharge time in seconds, m for active materials mass (g), and Δv for the potential window (V).

S.3 Fabrication of Asymmetric Supercapacitor (ASC) Device (Two-Electrode System)

The positive and negative electrodes, as well as the 6 M KOH electrolyte, were provided by an asymmetric supercapacitor device configured as CNT-Ni-Cu-Ag/KOH/activated carbon (AC). The active material/AC: PVDF: carbon black (80:10:10) was first ground, and NMP solvent was added while grinding to generate a slurry that was then utilised to make the positive electrodes. To prepare the negative electrode, the ratio of AC: PVDF: NMP were mixed and ground until it became a good slurry. The anode and cathode were separated using a glass microfibre separator before being assembled into a sandwich-style configuration. As a result, the ASC device was used and its performance assessed. Additionally, other SC parameters (specific capacitance, power, energy densities, etc.) from both SC and GCD investigations were examined, as well as the mass balancing/loading of the electrodes.

S.4 Photocatalytic degradation measurement

To evaluate the photocatalytic degradation capabilities of the newly synthesized visible light-activated catalyst, Diclofenac and Ciprofloxacin were utilized as representative organic pollutants. For the establishment of adsorption and desorption equilibrium of organic pollutants on the catalyst surface, 25 mg of the catalyst was introduced into 50 mL of an aqueous organic pollutants with a concentration of 20 g L^{-1}, and the solutions were kept in the absence of light. Subsequently, 2 mL of the solution was extracted at specified intervals after subjecting the organic pollutants solution to visible light exposure for 2 h. Furthermore, post-centrifugation, the solutions were filtered using a 0.22 µm syringe filter. The determination of the degradation

efficiency of the organic pollutants was conducted by measuring the decomposition using a UV-Vis spectrophotometer. Degradation efficiency is determined using the following Eqn **3**.

$$Efficiency\,\% = \frac{C_0 - C}{C_0} \times 100 \quad (3)$$

where C_0 and C are the dye pollutant's starting and final concentrations, respectively. The catalyst was then removed from the first photocatalytic reaction using a centrifuge, rinsed with ethanol/water (10% v/v), and dried at 80°C. By degrading the dye pollutant, the regenerated catalyst was used to determine its stability and reusability.

The following Eqn **4** on the appropriate rate of Diclofenac and Ciprofloxacin degradation was drawn using first-order kinetic reaction values:

$$-\ln(C/C_0) = kt \quad (4)$$

where t is time and k is the rate constant of the reaction. The investigation into photocatalytic degradation took visible light (Xe lamp) photoreactor, with abundant sunlight prevailing from 11:00 a.m. to 2:30 p.m. Throughout each experiment, the recorded average solar light intensity was 1.10 x 10^5 lux.

S.5 Instrumentation

Powder X-ray diffraction (PAN Analytical X'pert PRO Model X-ray diffractometer) with a monochromatic source of Cu-Kα-1 (λ=1.5418 Å) was used to confirm the prepared samples. To investigate the functional groups in the samples, Fourier transform infrared (FT-IR) analysis was performed using a Bruker Optik GmbH TENSOR-27 model spectrophotometer. The surface morphology was assessed using a FE-SEM (JEOL JSM-6700F) model operating at 10 and 30 kV. Transmission electron microscopy (TEM, JEM 2100 F) was used to analyse the morphology of the produced samples at a high magnification range at a voltage of 200 kV. To evaluate the bandgap of the samples, the reflectance was measured by Diffuse reflectance spectra UV-Vis spectroscopy and the photocatalytic dye degradation

solution samples were analysed by a UV/Vis double beam spectrophotometer (VARIAN, Cary 5000) in the wavelength range of 200–800 nm. A Raman spectrum was acquired using a Renishaw Raman microscope equipped with a 532 nm laser wavelength. The XPS analysis conducted on a PHI5000 version Probe III determined the valences of the elements found in the samples.

All theoretical calculations are carried out within the framework of density functional theory (DFT) using the B3LYP functional in combination with the 6-31G basis set. Within the DFT approach, the electronic structure and total energy of a multi-electron system are determined as functionals of the electron density, enabling an accurate and computationally efficient description of the system's quantum-mechanical properties.

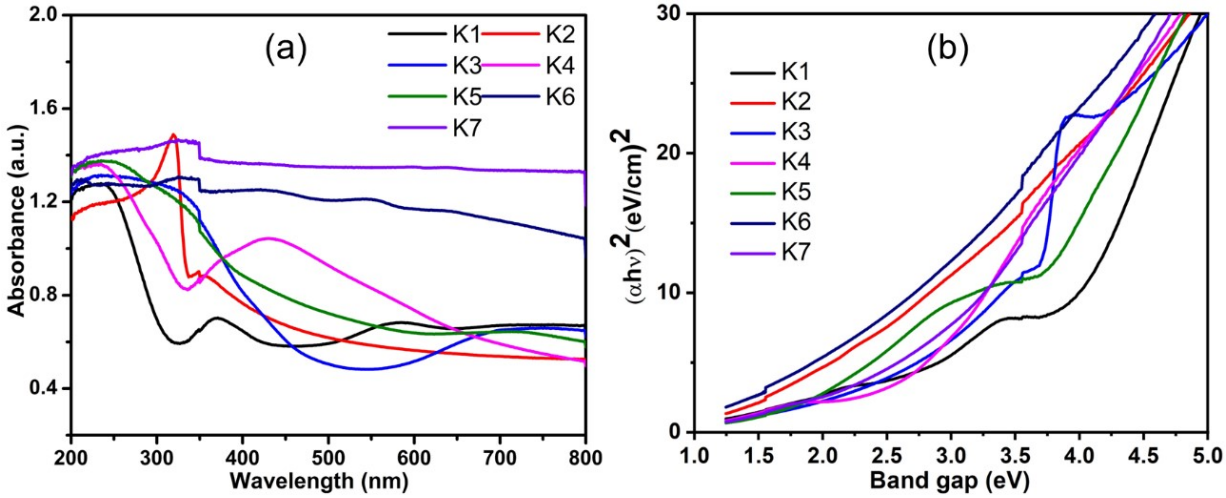

Figure. S1. Shows **(a)** UV-Vis's absorbance spectrum and **(b)** band gap of K1-CNT-Ni, K2-CNT-Cu, K3-CNT-Ag, K4-CNT-Ni-Cu, K5-CNT-Ni-Ag, K6-CNT-Cu-Ag and K7-CNT-Ni-Cu-Ag samples.

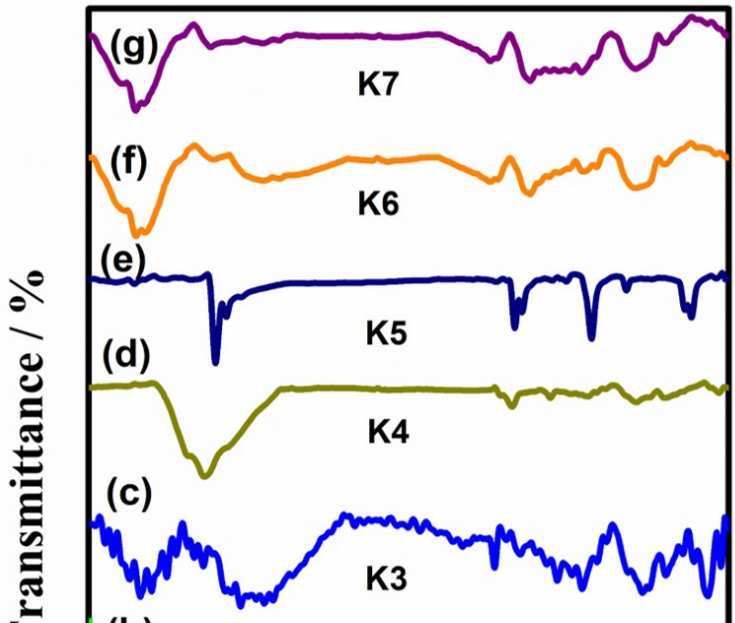

Figure. S2(a-g). Shows FTIR spectrum of K1-CNT-Ni, K2-CNT-Cu, K3-CNT-Ag, K4-CNT-Ni-Cu, K5-CNT-Ni-Ag, K6-CNT-Cu-Ag and K7-CNT-Ni-Cu-Ag samples.

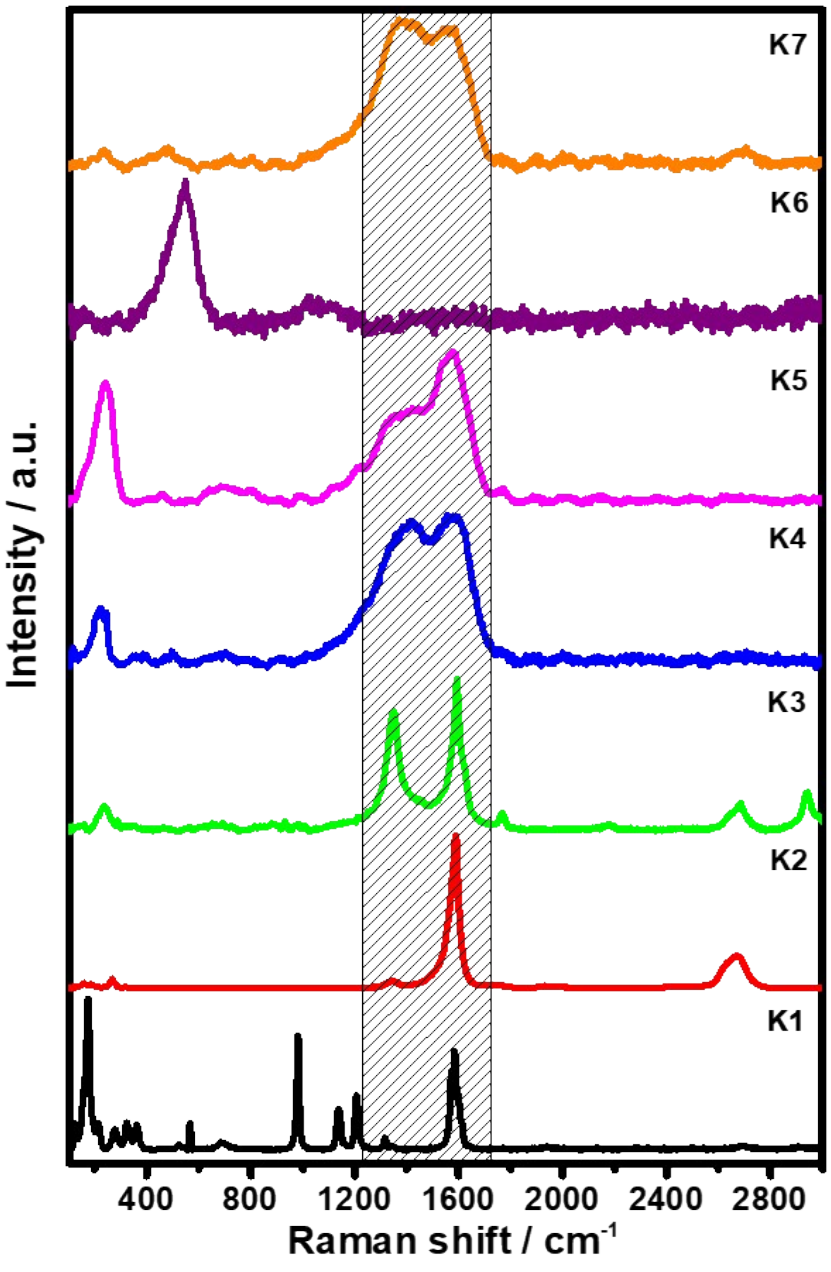

Figure. S3. Raman spectrum of K1-CNT-Ni, K2-CNT-Cu, K3-CNT-Ag, K4-CNT-Ni-Cu, K5-CNT-Ni-Ag, K6-CNT-Cu-Ag and K7-CNT-Ni-Cu-Ag samples.

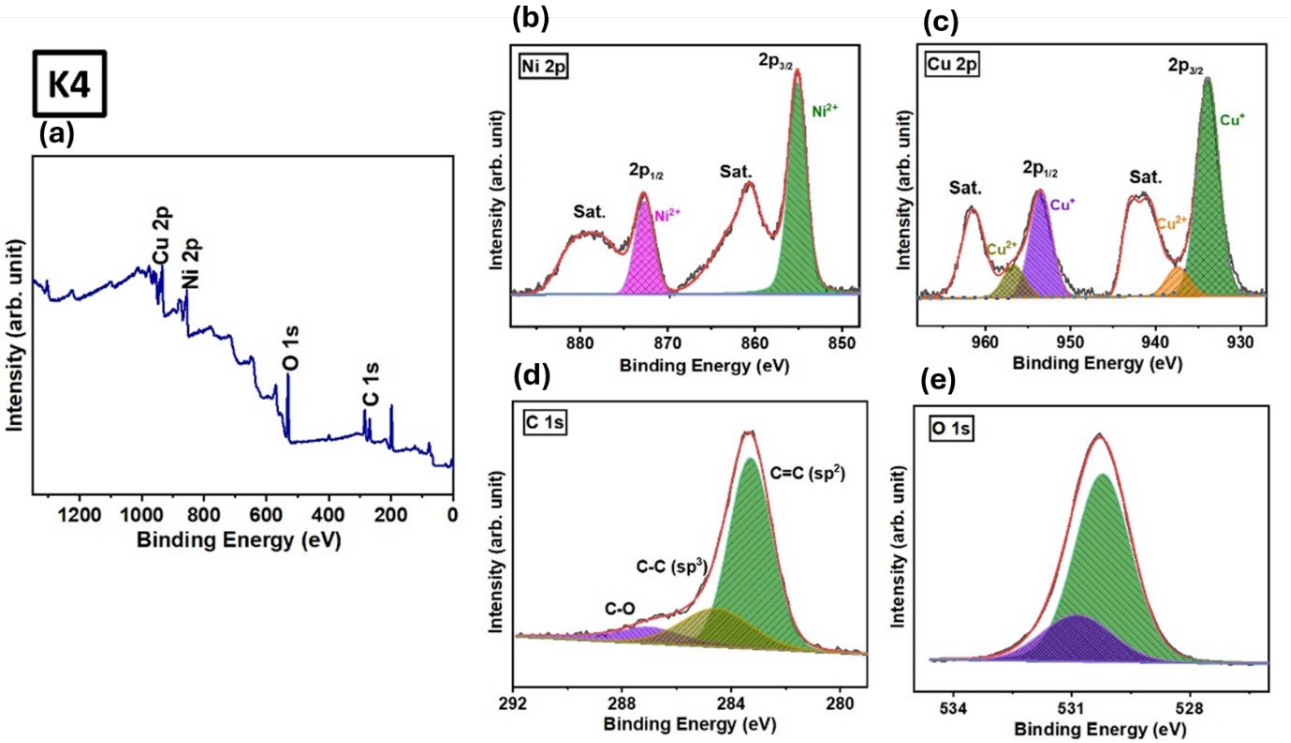

Figure. S4. (a) XPS survey spectra of K4 (CNT-Ni-Cu) **(b-e)** show the high-resolution spectra of Ni 2p, Cu 2p, C 1s and O 1s, respectively.

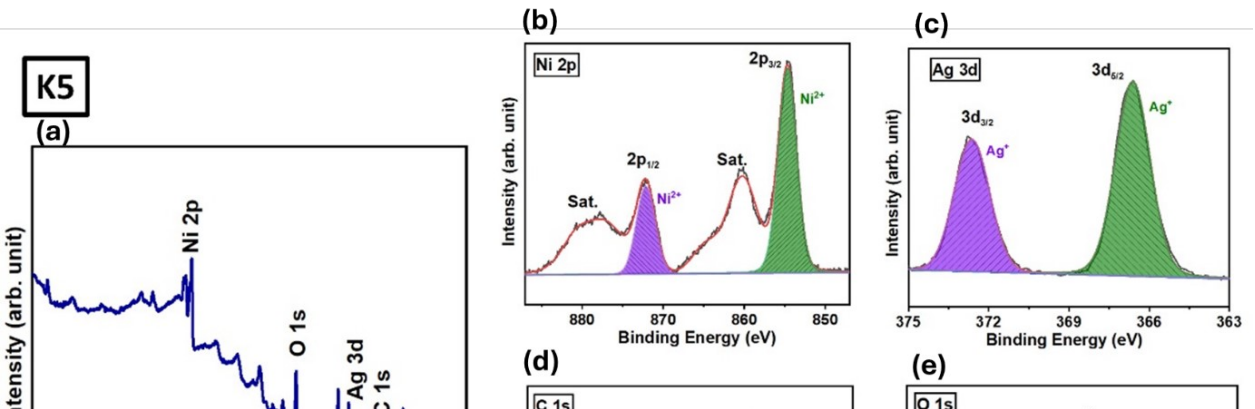

Figure. S5. (a) XPS survey spectra of K5 (CNT-Ni-Ag) **(b-e)** show the high-resolution spectra of Ni 2p, Ag 3d, C 1s and O 1s, respectively.

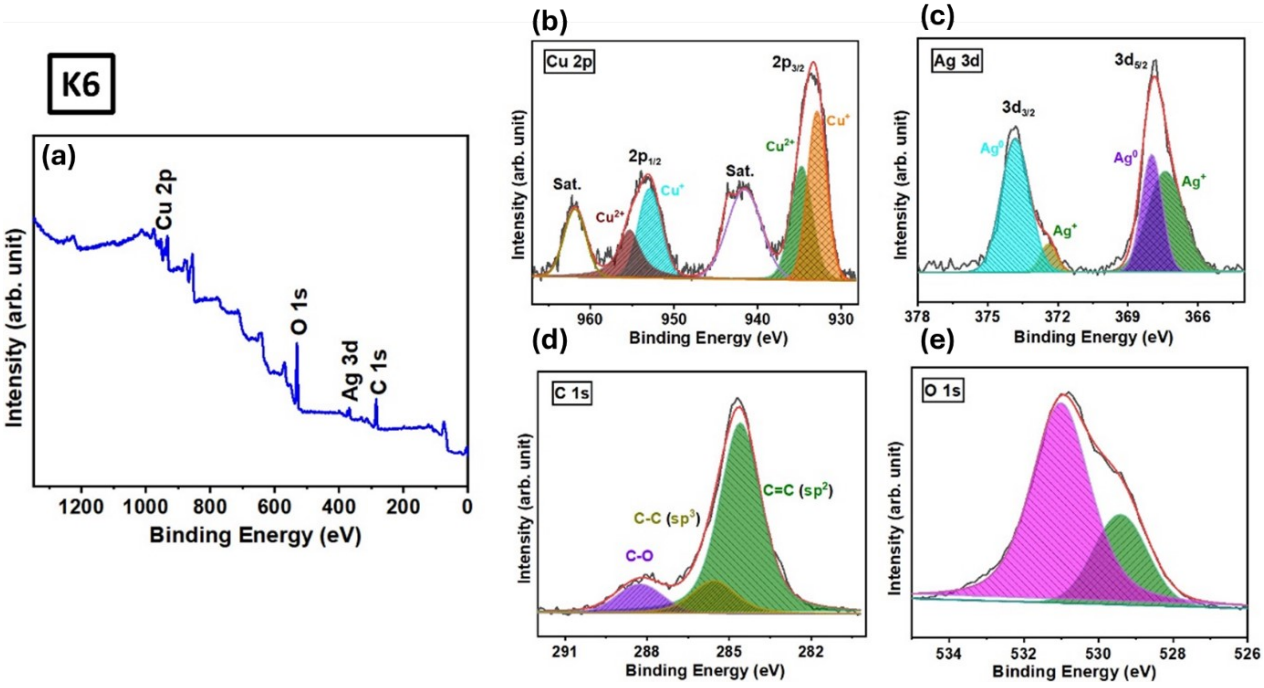

Figure. S6 (a) XPS survey spectra of K6 (CNT-Cu-Ag) **(b-e)** show the high-resolution spectra of Cu 2p, Ag 3d, C 1s and O 1s, respectively.

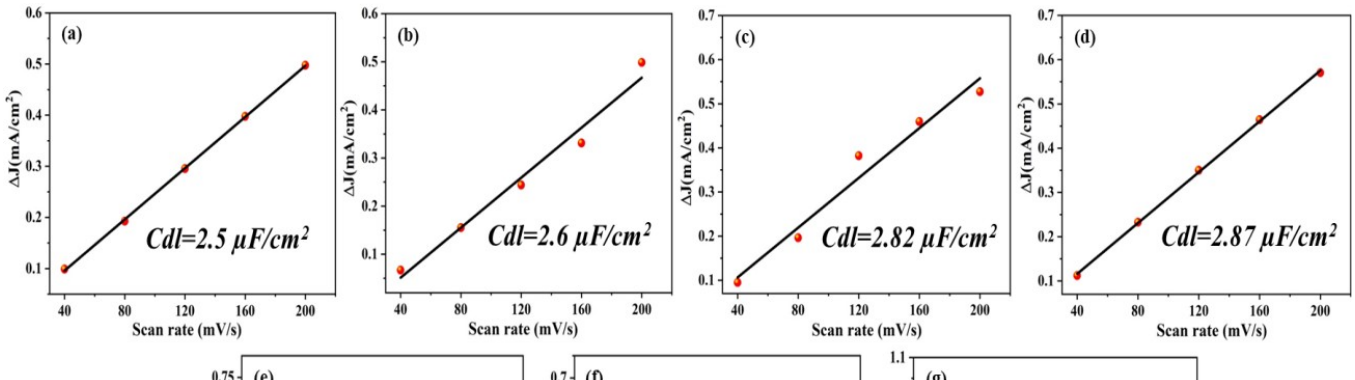

Figure. S7. (a-g) Different scan rate vs. current density plot of K1-K7 nanocomposites

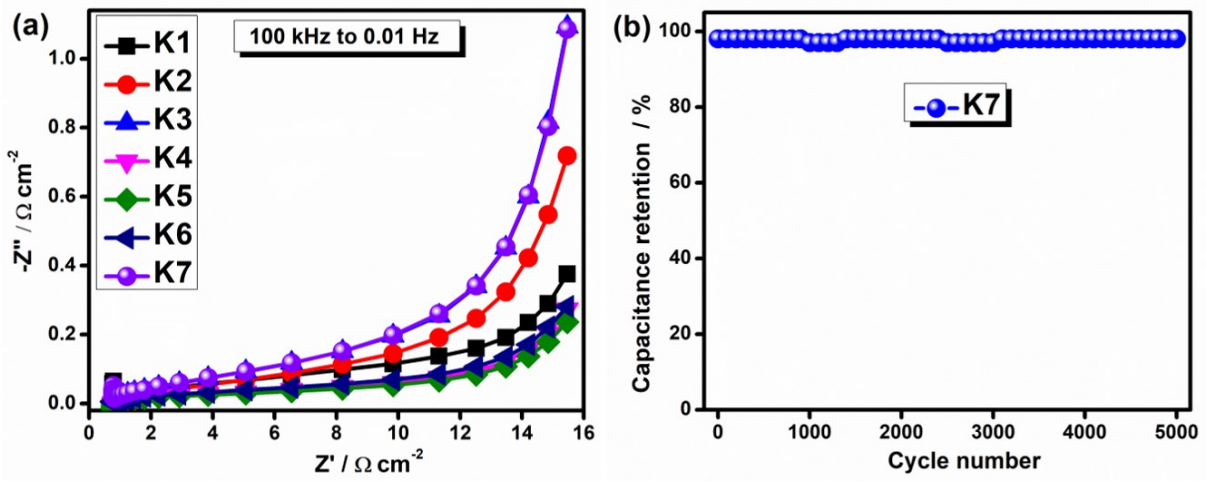

Figure. S8 (a) Nyquist plots of all electrodes are illustrated, and **(b)** Cycling stability performance of the K7 electrode and a Schematic diagram of the Supercapacitor.

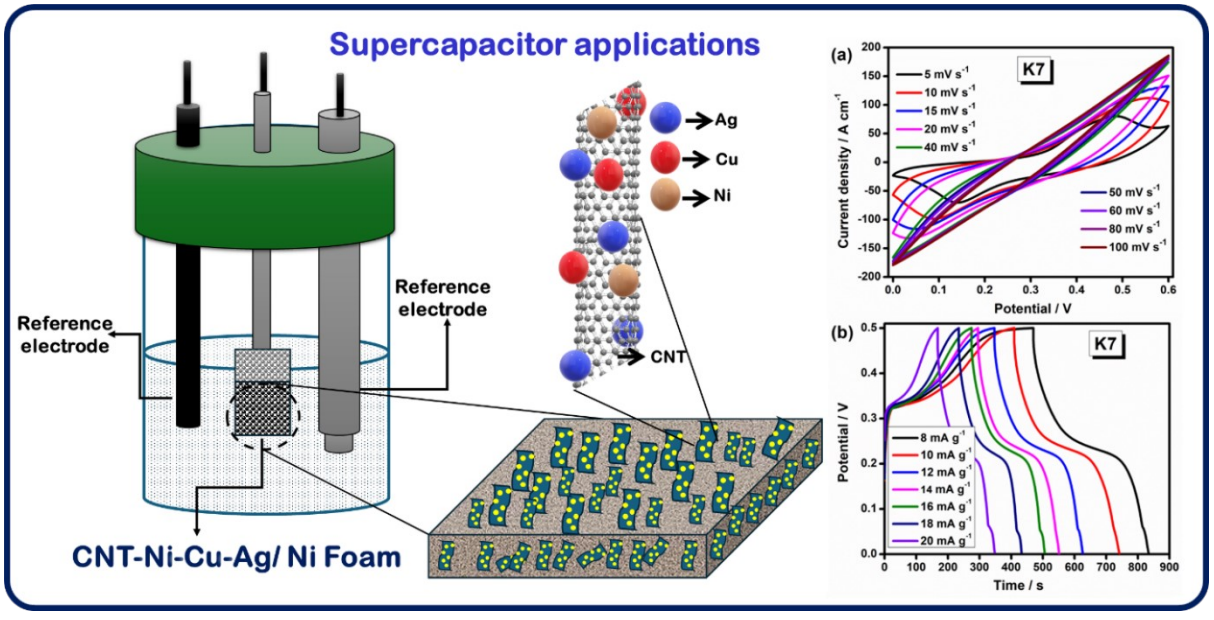

Figure. S9 Represent the electrochemical performance of the K7 electrode.

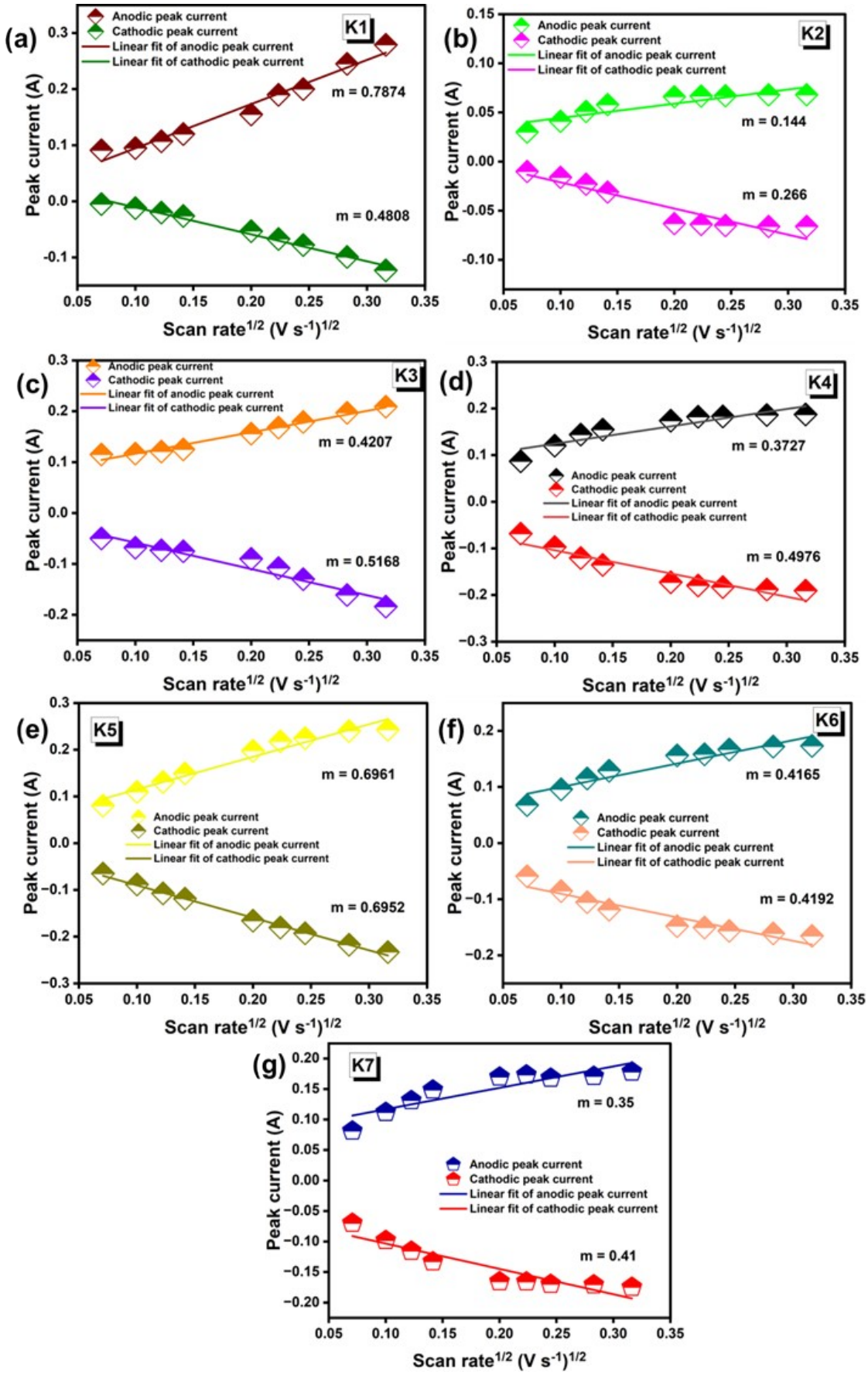

Figure. S10 Randles Sevcik plot from CV curves of K1-CNT-Ni, K2-CNT-Cu, K3-CNT-Ag, K4-CNT-Ni-Cu, K5-CNT-Ni-Ag, K6-CNT-Cu-Ag and K7-CNT-Ni-Cu-Ag samples.

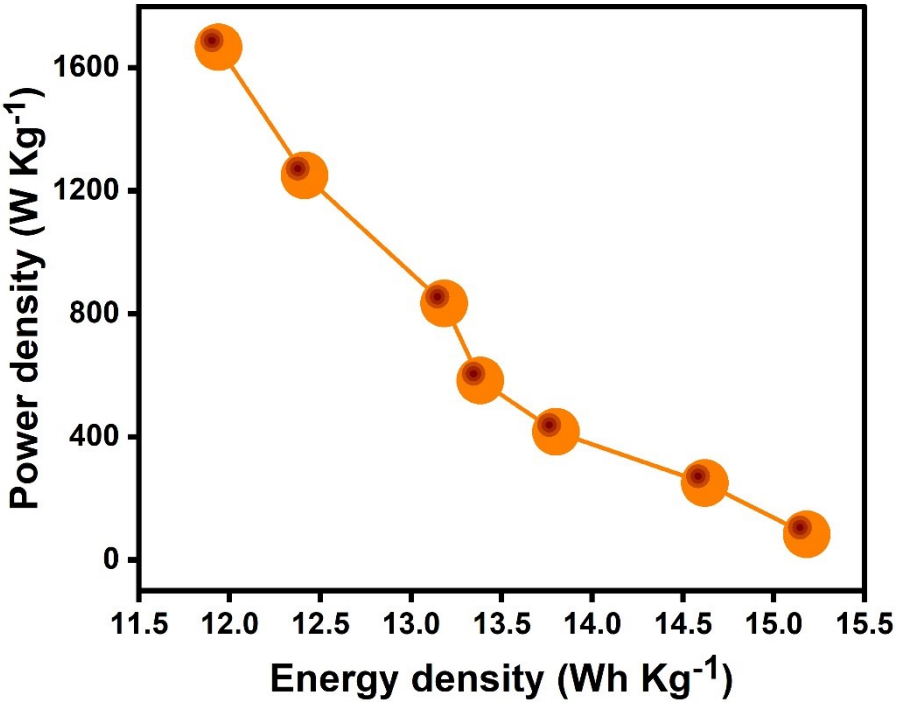

Figure. S11 Ragone plot of fabricated ASC device

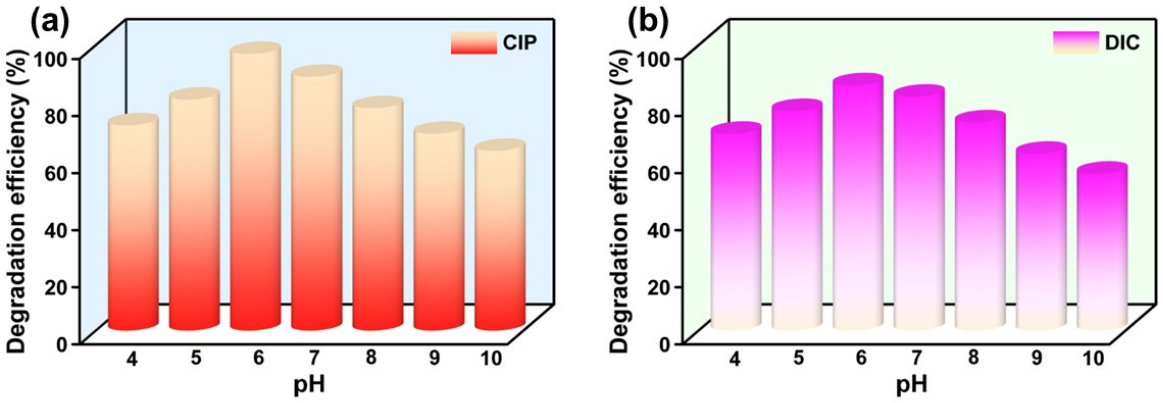

Figure. S12 Effect of pH on photocatalytic degradation of **(a)** CIP and **(b)** DIC for the K7 nanocomposites.

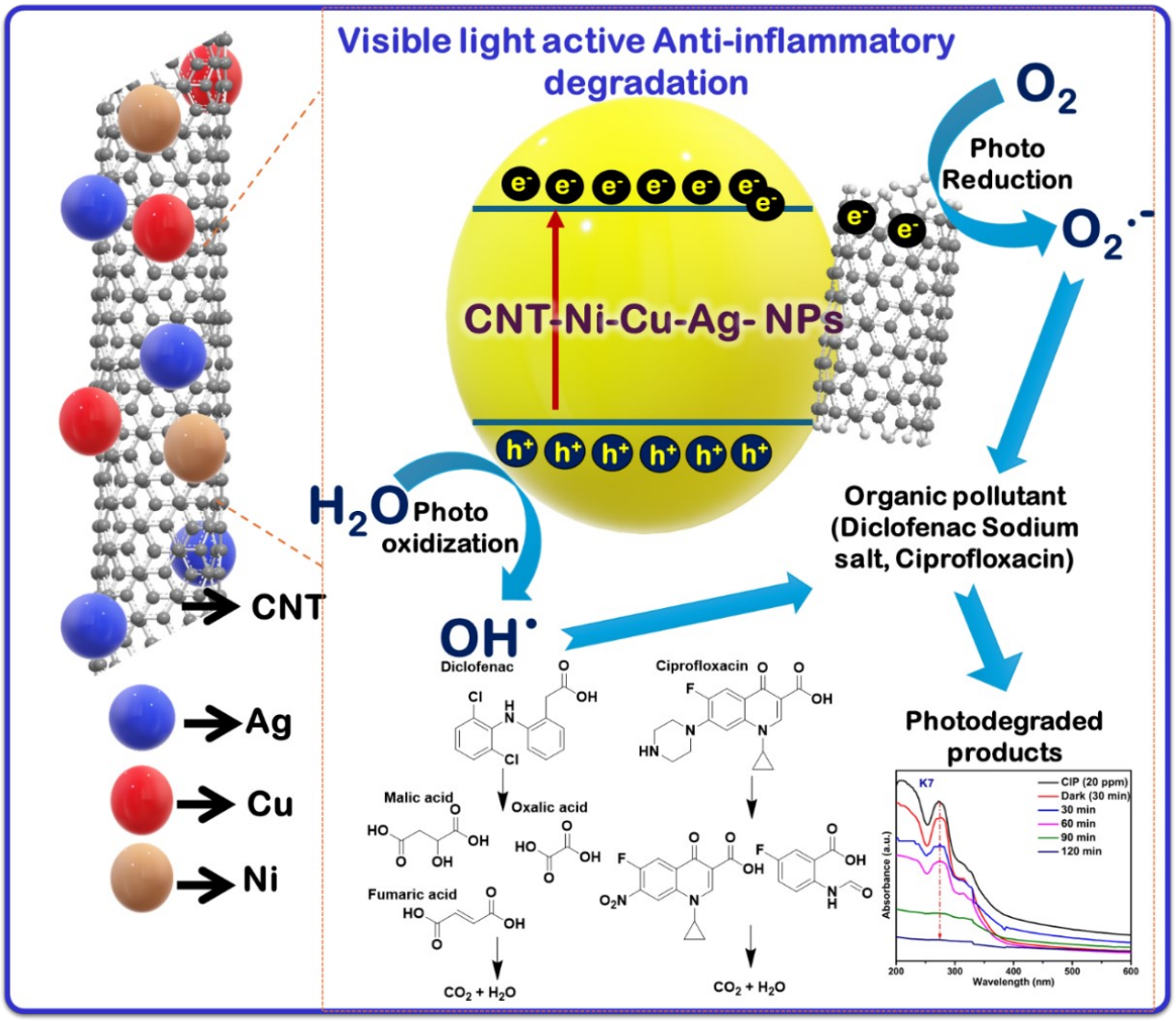

Figure. S13: Represent the photocatalytic mechanism of K7 against DIC and CIP solution.

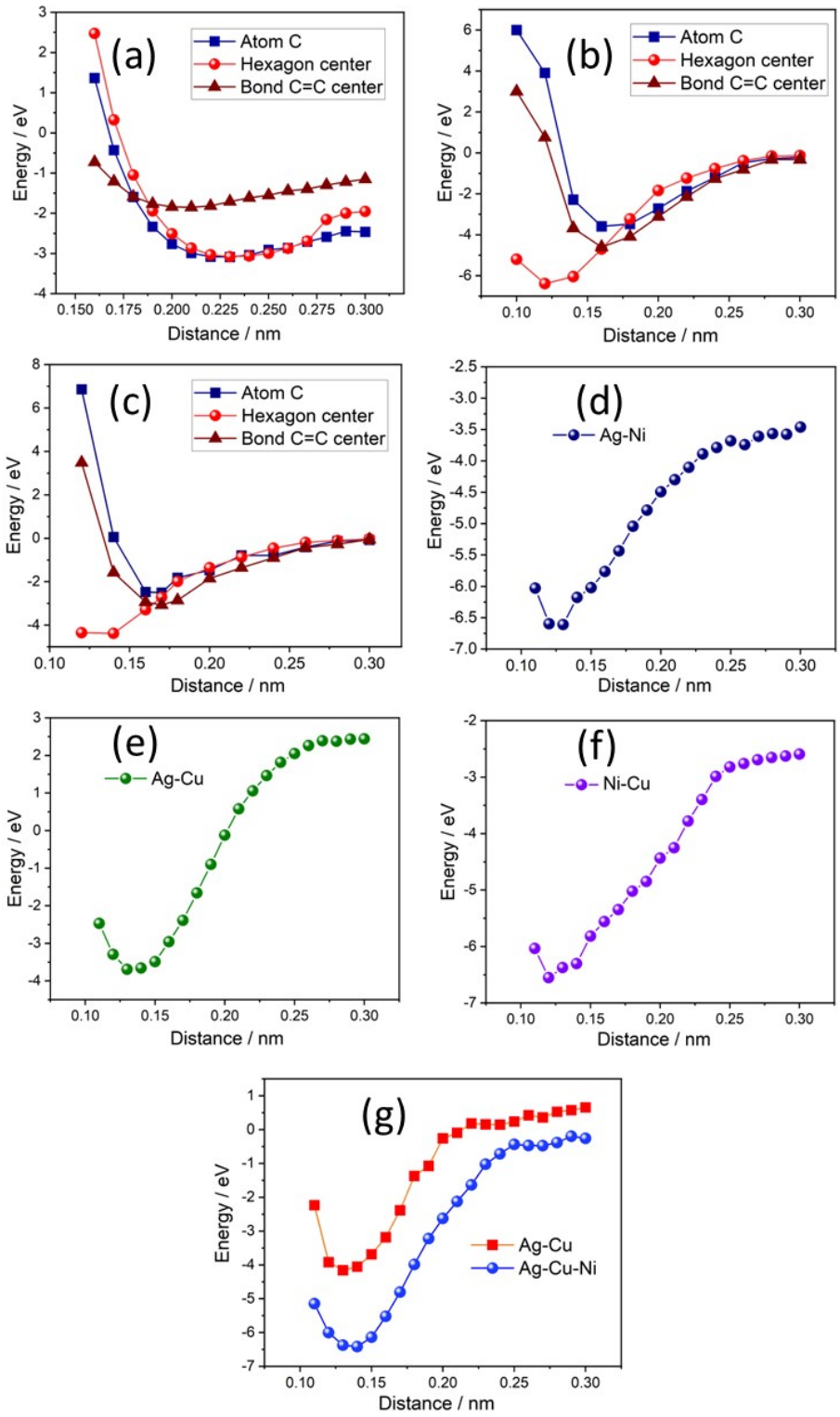
(a)
Atom C
Hexagon center
Bond C=C center
Energy / eV
Distance / nm
(b)
Atom C
Hexagon center
Bond C=C center
Energy / eV
Distance / nm
(c)
Atom C
Hexagon center
Bond C=C center
Energy / eV
Distance / nm
(d)
Ag-Ni
Energy / eV
Distance / nm
(e)
Ag-Cu
Energy / eV
Distance / nm
(f)
Ni-Cu
Energy / eV
Distance / nm
(g)
Ag-Cu
Ag-Cu-Ni
Energy / eV
Distance / nm

Figure. S14 Potential energy surface profiles on the position of atoms relative to the surface of the nanotube: **(a-c)** The dependence of energy on distance for three variants of the location of the Ag, Ni and Cu atoms: above the carbon atom, above the C-C bond centre and above the centre of the hexagon, respectively. **(d-f)** The dependence of the energy value on the position of a pair of Ag-Ni, Ag-Cu and Ni-Cu atoms, respectively. **(g)** The dependence of the energy value during the triple attachment of atoms to different sides of the nanotube: stage 1 - approximation of the Cu atom; stage 2 - approximation of the Ni atom.

Table. S1 Number of graphene layers depends on I_D/I_G ratio

S. No.	Sample	I_D	I_G	I_D/I_G
1	K1 – CNT-Ni	1527	7636	0.20
2	K2 – CNT-Cu	4091	42294	0.10
3	K3 – CNT-Ag	4500	6105	0.74
4	K4 – CNT-Ni-Cu	4500	4909	0.92
5	K5 – CNT-Ni-Ag	8400	15000	0.56
6	K6 – CNT-Cu-Ag			
7	K7 – CNT-Ni-Cu-Ag	5680	5332	1.07

Table. S2 XPS binding energy values of elements C, O, Ni, Cu and Ag for the composites K4-K7.

Elements	K4			K5			K6			K7		
Carbon (eV)	283.3	284.6	287.0	283.2	284.2	286.7	284.7	285.5	288.2	283.6	284.4	286.8
Oxygen (eV)	530.2	530.9	-	529.8	531.2	-	529.4	531.0	-	530.3	532.2	-
Nickel (eV)	855.2	872.7	-	854.7	872.1	-	-	-	-	855.4	873.0	-
Copper (eV)	933.8 937.4	953.5 956.6	-	-	-	-	932.9 934.8	952.9 955.2	-	933.3 935.0	953.6 957.3	-
Silver (eV)	-	-	-	366.6	372.6	-	367.4 368.0	372.4 373.8	-	366.4	372.5	-

Table. S3 Comparison of the specific capacitance with the previous literature

Electrode material	**Preparation method**	**Electrolyte**	**Specific capacitance ($F\ g^{-1}$)**	**Current density ($A\ g^{-1}$)**	**Retention (%)**	**Cycles (numbers)**	**Ref**
CNT@Mn-MOF	Hydrothermal process	Na_2SO_4	203	1	88	3000	[39]
CNT/Ag cellulose acetate membrane	-	1 M Na_2SO_4	72.8 F/cm^3	0.5 mA/cm^2	75.92	1000	[40]
CNT/ZnO	Chemical reflux method	1 M Na_2SO_4	189	1 mVs^{-1}	96	1000	[41]
CNT/ZnO	Spray pyrolysis	PVA/PMA	126.3	-	-	-	[42]
CNT/GT/ZnO	Sol-Gel method	1 M KCL	6.99	5 mVs^{-1}	-	-	[43]
MnO_2@MXene/CNT	Hydrothermal	Na_2So_4	181.8	1	91	5000	[58]
ZnO/ MWCNT	Hydrothermal	1 M Tetraethyl ammonium tetra fluoroborate	40	5 mVs^{-1}	-	1000	[45]
MWCNTf-ZnS	Facile method	6 M KOH	95	-	85	4000	[48]
MnO_2/CNT	Chemical vapour deposition	3 M KCL	540	5	56	1000	[47]
Binder-free activated carbon/ CNT	-	6 M KOH	267	200 mVs^{-1}	97.5	5000	[49]
CNT/NiO	Hydrothermal	6 M KOH	713.9	2 mVs^{-1}	88.2	3000	[50]
CNT/NiS/CoS			1249	1	97.17	8000	[46]
rGO/CNT	Chemical vapour deposition	1 M Na_2SO_4	151	0.5	86	6000	[44]
CNT@$Ni(OH)_2$	Chemical bath deposition	1 M KOH	1136	2	92	1000	[51]
MnO_2-CNT/Ni	Chemical rection	0.5 M Na_2SO_4	402.5	1	83	5000	[52]
CNT/$Ni(OH)_2$	Hydrothermal	3 M KOH	912.22	10mVs^{-1}	84	1000	[53]
MWCNTs/IL/Mn	Chemical reduction method	3 M KOH	432.4	5 mVs^{-1}	90	1000	[54]

$Mn(MnO)/Mn_5C_2$/CNT	Chemical vapor deposition	0.5 M Na_2SO_4	378.9	2 mVs^{-1}	-	1000	[55]
CNT/MnO_2	Chemical method	1 M Na_2SO_4	145.6	5 mVs^{-1}	98	1500	[56]
MnO_2/CNT	Solid-state microwave method		1250	1	80	7000	[57]
CNT-Ni-Cu-Ag	Hydrothermal	6 M KOH	1451	8	99	5000	This work

Table. S4 Comparison of the photocatalytic activity with the previous literature

S.No	Catalyst	Pollutant	Conc	Dose Mg/L	Source	Efficiency (%)	Duration	Reference
1.	Fe_3O_4 /MWCNT	Diclofenac	10 ppm	100	-	95.0	180	[66]
2.	PVDF/MWCNT	Diclofenac	12.5	-	Visible light	95.0	240	[67]
3.	(δFeOOH)/MWCNT	Ciprofloxacin	10 ppm	23.5	UV	86.9	131.6	[68]
4.	Ag_2O/Ag_2CO_3/MWNT	Ciprofloxacin	10 ppm	0.05g	Visible	76.0	-	[69]
5.	Bi_2WO_6/MWCNT	Ciprofloxacin	10 ppm	-	UV	91.3	120	[70]
6.	Fe_3O_4/ MWCNT	Ciprofloxacin	150 PPM	30	Visible light	78.0	-	[71]
7.	MWCNT	Ciprofloxacin	8 PPM	1.77	Visible light	88.0	240	[72]
8.	Fe_3O_4 /MOF/AmCs-Alg	Ciprofloxacin	10 ppm	400	Visible light	95.8	-	[73]
9.	O-g-C_3N_4/ZnO/TiO_2	Diclofenac	10 ppm	100	UVA light	35.1	50	[74]
10.	MWCNT	Diclofenac	10 ppm	80	-	97.8	120	[75]
11	CNT-Ni-Cu-Ag	Diclofenac	20 ppm	250	Visible light	86.0	120	This work
12	CNT-Ni-Cu-Ag	Ciprofloxacin	20 ppm	250	Visible light	98.5	120	This work

Table. S5 The main parameters of the interaction of CNTs (6, 0) with metal atoms: r - interaction distance, nm, E - interaction energy, eV, ΔEg - band gap in eV.

Metal atoms	r, nm	E,	ΔE_g, eV
Ag	0.23	-3.09	0.28
Ni	0.12	-6.39	0.58
Cu	0.14	-4.38	0.31
Ag-Ni	0.13	-6.61	0.51
Ag-Cu	0.13	-3.69	0.3
Ni-Cu	0.12	-6.55	0.57
Ag-Cu, 120^0	0.13	-4.16	0.31
Ag-Ni-Cu	0.14	-6.42	0.36
CNT (6, 0) without metals			0.69

Table S6. Charges (Q) on the atoms of the complexes "CNT (6, 0) + metal atoms"

Atomic complexes		Q_{Me}	The charge of the nearest carbon neighbors
(6, 0)+Ag		0.642	-0.068
(6, 0)+Ni		0.881	-0.132
(6, 0)+Cu		0.574	-0.109
(6, 0)+Ag-Ni	Ag	0.406	-0.052
	Ni	0.804	-0.158
(6, 0)+Ag-Cu	Ag	0.387	-0.052
	Cu	0.806	-0.157
(6, 0)+Ni-Cu	Ni	0.806	-0.106
	Cu	0.802	-0.149
(6, 0)+Ag-Ni-Cu	Ag	0.376	-0.055
	Cu	0.801	-0.157

	Ni	0.802	-0.157